

Phase Detection with Neural Networks: Interpreting the Black Box

Anna Dawid,^{1,2} Patrick Huembeli,² Michał Tomza,¹ Maciej Lewenstein,^{2,3} and Alexandre Dauphin²

¹*Faculty of Physics, University of Warsaw, Pasteura 5, 02-093 Warsaw, Poland*

²*ICFO-Institut de Ciències Fotòniques, The Barcelona Institute of Science and Technology, Av. Carl Friedrich Gauss 3, 08860 Castelldefels (Barcelona), Spain*

³*ICREA, Pg. Lluís Companys 23, 08010 Barcelona, Spain*

(Dated: April 26, 2022)

Neural networks (NNs) normally do not allow any insight into the reasoning behind their predictions. We demonstrate how influence functions can unravel the black box of NN when trained to predict the phases of the one-dimensional extended spinless Fermi-Hubbard model at half-filling. Results are the first indication that the NN correctly learns an order parameter describing the transition. Moreover, we demonstrate that influence functions not only allow to check that the network trained to recognize known quantum phases can predict new unknown ones but even discloses information about the type of phase transition.

Machine learning (ML) influences everyday life in multiple ways with applications like letter and voice recognition software, fingerprint identification, e-mail spam filtering, self-driving cars, and many others. These versatile algorithms, dealing with big and high-dimensional data, also have a prominent impact on science, as neural networks (NNs) have been harnessed to solve problems of quantum chemistry, material science, and biology [1–4]. Physics is no different in exploring ML methods, encompassed already by astrophysics, high-energy physics, quantum state tomography, and quantum computing [5–11]. Especially abundant is the use of ML in phase classification which is not surprising if one considers that determining the proper order parameters for unknown transitions is no trivial task, on the verge of being an art. It includes the search in the exponentially large Hilbert space and the examination of symmetries existing in the system, guided by the intuition and educated guess. The alternative route was shown, when NNs, used commonly for high-dimensional data analysis, located the phase transitions for known systems without a priori physical knowledge [12, 13]. However, the resulting models were agnostic, largely opaque, and ‘intelligence’ was provided by extracting it from data, which is in stark contrast with a physicists’ main driving force: the need to understand the underlying mechanisms of the process. At the same time, it is undeniable that ML often produces surprisingly good results.

Deep fully connected and convolutional neural networks (CNN) have been applied to detect phase transitions in a variety of physical models, for classical [12, 14–16], quantum [13, 17–23], and topological phase transitions [24–28] with supervised [12, 18, 21, 26, 27, 29] and unsupervised [13, 14, 17, 20, 22, 23, 28] approaches. Other examples include ML models that do not leverage deep architectures [30, 31].

Next to all these successful applications, there are open problems, for instance ones concerning topological models and many-body localization (MBL), which include the need for pre-engineered features [32–34], disagreement of predicted critical exponents [19], and high sensitivity to hyperparameters describing the training pro-

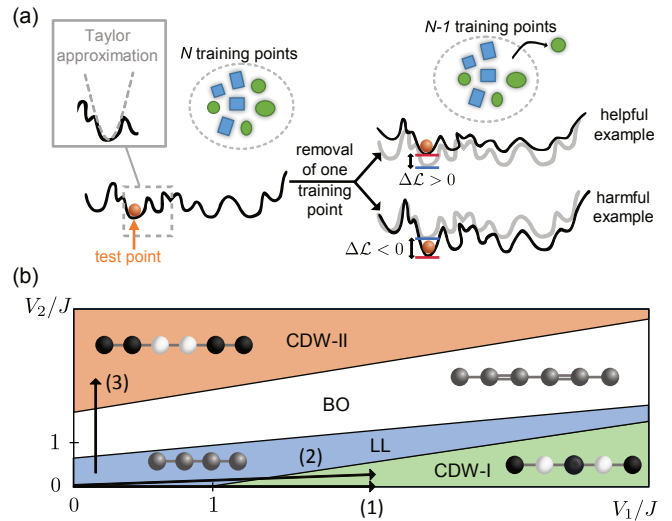


FIG. 1. (a) Visual explanation of leave-one-out training and its approximation, the influence function. (b) Schematic phase diagram of the extended one-dimensional half-filled spinless Fermi-Hubbard model with the schemes of the corresponding states: LL - Luttinger liquid, BO - bond order, CDW-I and II - charge density wave type I and II. The arrows indicate the transitions studied in this work.

cess [21]. Moreover, even in the models described by Landau’s theory, so far, these approaches have mostly enabled only the recovery of known phase diagrams or the location of phase transitions in qualitative agreement with more conventional approaches based, for instance, on order parameters and/or theory of finite-size scaling. Nonetheless, ML achieved this at a much lower computational cost, e.g. using fewer samples or smaller system sizes [19, 21].

Additionally, used ML techniques are mostly black boxes, i.e., systems with internal logic not obvious at all to a user [35]. The missing key element is the model interpretability, i.e., the ability to be explained or presented to a human in understandable terms [36]. The research on this crucial property is at heart of a booming field of ML interpretability [37–42] aiming at designing methods that discover the internal logic of commonly used black boxes.

They are needed for a plethora of reasons. Given the ML presence in everyday life, it is no surprise that already legal measures have been taken to assure that any individual can obtain meaningful explanations of the logic involved when automated decision-making takes place [43]. Next to the legal motivations, there is ethics. The worrying fact was revealed that learning machines inherit biases from humans preparing data [44]. Also, deep NNs were shown to perfectly fit random labels [45], and that a group of local features can be their good approximation [46]. These studies prove that the learning process sometimes goes against our intuition, and indicate that the predictions should be accompanied by a justification understandable by humans to be trusted.

Moreover, an overwhelming need for ML interpretability was born after first successful uses of ML in physics. Its numerical power cannot be denied, but its frequent automatic use contradicts the primary motivation of physical research, namely the desire to know and understand the underlying mechanisms of the process. Instead, with black boxes, we stop at reproducing the process. Even in phase classification problems, where NNs have been often used, we cannot be fully confident that NNs learn order parameters. Hence, in this work, we show how interpretability methods can be used in the classification of physical phase transitions to understand what characteristics are learned by a ML algorithm. This approach unravels if a relevant physical concept was indeed learned or if the prediction cannot be trusted. We also present that interpretable NN can give additional information on the phase transitions, not provided to the algorithm explicitly.

Supervised learning. We consider supervised learning problems with labeled training data $\mathcal{D} = \{z_i\}_{i=0}^n$, with $z_i = (x_i, y_i)$. The input data is coming from some input space $x_i \in \mathcal{X}$, and the model predicts the outputs coming from some output space $y_i \in \mathcal{Y}$. In our setup, the inputs x_i are the state vectors for a given physical system, and y_i are the corresponding phase labels. The model is determined by the set of parameters θ . In the training process, the parameters' space is being searched for the final parameters $\hat{\theta}_{\mathcal{D}} \equiv \hat{\theta}$ of the ML model, which minimize the training loss function $\mathfrak{L}(\mathcal{D}, \theta) = \frac{1}{n} \sum_{z \in \mathcal{D}} \mathcal{L}(z, \theta)$, where n is the training data set size, which tends to be of the order of thousands. After training, a model can make a prediction for an unseen test point z_{test} with the test loss function value $\mathcal{L}(z_{\text{test}}, \hat{\theta})$ related to the model certainty of this prediction.

Interpreting neural networks. An intuitive way of unraveling the logic learned by the machine is retraining the model after removing a single training point z_r (starting from the same minimum, if a non-convex problem is analyzed), and checking how it changes the prediction of a specific test point z_{test} . Such a leave-one-out training (LOO) [47] studies the change of the parameters θ , now shifted to a new minimum $\hat{\theta}_{\mathcal{D} \setminus \{z_r\}}$ of the loss function, as depicted in Fig. 1(a). An analysis of the test loss change, $\Delta\mathcal{L} \equiv \mathcal{L}(z_{\text{test}}, \hat{\theta}) - \mathcal{L}(z_{\text{test}}, \hat{\theta}_{\mathcal{D} \setminus \{z_r\}})$, enables the indica-

tion of the most influential training points for a given test point z_{test} being the ones whose removal causes the largest change. Influential examples can be both helpful ($\Delta\mathcal{L} > 0$) and harmful ($\Delta\mathcal{L} < 0$). Such an analysis gives the notion of a similarity used by the machine in a given problem, as training points being the closest in the $\Delta\mathcal{L}$ space can be understood as the most similar. Once the most influential points are indicated, we can decode what characteristics are being looked at by comparing 'similar' points in the machine 'understanding'. It can be especially useful in phase classification problems where the analysis of $\Delta\mathcal{L}$ enables the recovery of patterns being crucial for distinguishing the phases. The use of this technique to check the influence of every training point in \mathcal{D} on a given test point is, however, prohibitively expensive, as the model has to be retrained for each removed z .

To circumvent this problem, one can make a Taylor expansion of the loss function \mathcal{L} with respect to the parameters around the minimum $\hat{\theta}$, and approximate $\Delta\mathcal{L}$ resulting from the LOO training. This method was proposed for regression problems already forty years ago [47–49] and named influence functions. Not only this interpretability method is computationally feasible, but also it treats a model as a function of the training data instead of assuming that the training data set is fixed. The influence function reads

$$\mathcal{I}(z_r, z_{\text{test}}) = \frac{1}{n} \nabla_{\theta} \mathcal{L}(z_{\text{test}}, \hat{\theta})^T H_{\theta}^{-1}(\hat{\theta}) \nabla_{\theta} \mathcal{L}(z_r, \hat{\theta}),$$

and it estimates $\Delta\mathcal{L}$ for a chosen test point z_{test} after the removal of a chosen training point z_r . $\nabla_{\theta} \mathcal{L}(z_{\text{test}}, \hat{\theta})$ is the gradient of the loss function of the single test point, $\nabla_{\theta} \mathcal{L}(z_r, \hat{\theta})$ is the gradient of the loss function of the single training point whose removal's impact is being approximated, and $H_{\theta}^{-1}(\hat{\theta})$ is the inverse of Hessian, $H_{i,j}(\hat{\theta}) = \frac{\partial^2}{\partial \theta_i \partial \theta_j} \mathfrak{L}(\mathcal{D}, \theta)|_{\theta=\hat{\theta}}$. All derivatives are calculated w.r.t. the model parameters θ , evaluated at $\hat{\theta}$ corresponding to the minimum of the loss, $\mathfrak{L}(\mathcal{D}, \hat{\theta})$. We can only ensure the existence of the inverse of the Hessian if it is positive-definite. However, it was shown [50, 51] that this method could be generalized to non-convex problems and therefore applied to ML. The example code can be found in [52].

Physical model. We apply influence functions to a small CNN (described in detail in appendix A) trained to recognize phases in the extended Hubbard model, namely a one-dimensional (1D) system consisting of spinless fermions at half filling with hopping between neighboring sites with amplitudes J , interacting with nearest neighbors with strength V_1 and next-nearest neighbors with strength V_2

$$\hat{H} = -J \sum_{\langle i,j \rangle} c_i^{\dagger} c_j + V_1 \sum_{\langle i,j \rangle} n_i n_j + V_2 \sum_{\langle\langle i,j \rangle\rangle} n_i n_j.$$

The competition between the system parameters J , V_1 , and V_2 leads to four different phases: gapless Luttinger

liquid (LL), two gapped charge-density-wave phases with density patterns 1010 (CDW-I) and 11001100 (CDW-II), and bond-order (BO) phase, as seen in Fig. 1(b) [53, 54]. The order parameter describing the transition to the CDW-I (-II) phase is the average difference between (next-)nearest-site densities, while the BO phase is characterized by staggered effective hopping amplitudes. Detailed description is included in appendix B. We feed the CNN with ground states expressed in the Fock basis, labeled with their appropriate phases, calculated for a 12-site system with QuSpin and SciPy packages [55, 56]. To lift the degeneracy of the ground state, we use guiding fields favoring one symmetry. We define the phase transition position where the order parameter's value is ten times larger than the corresponding guiding field (see appendix B). The hopping amplitude, J is set to 1 throughout the paper.

Transition between LL and CDW-I. We train a CNN to classify ground states into two phases: LL and CDW-I based on the transition line marked with the arrow (1) in Fig. 1(b) for $V_2 = 0$. We plot the influence functions of all training examples for a chosen test point (marked with orange line) in Fig. 2. The order parameter describing the transition here is the average difference between nearest-site densities, which is zero in the LL phase and non-zero (growing to one) in the CDW-I phase. The panels (a)-(b) present how influential training points are for test points from the LL phase. The test state (a) is the ground state located deeply in the LL phase, while (b) is closer to the transition.

If the CNN learns an order parameter, all training points, i.e., ground states from the LL phase exhibiting a zero order parameter, should be similarly positively influential, and that is exactly what we observe. They form an almost flat line in panels (a), (b), and (d). In panel (c), however, for the test point close to the transition, their influence changes linearly. This divergence from expected behavior is because in our exact diagonalization calculations, the order parameter in the LL phase is not exactly constant and equal to zero. Instead, it is growing very slowly, that is why finally the most helpful points are the ones near the transition - they are the most unique from the training points labeled as LL, and the information they provide is the most valuable. The nonzero order parameter is caused by three phenomena: the finite-size effect, use of the guiding fields, and the numerical arbitrariness of choosing the transition point. In the perfect scenario (observed, for example, for training on states obtained from mean-field calculations), the five most influential points should be randomly distributed over the whole LL phase. The most harmful training points are, in both cases, the ones closest to the transition, but on the CDW-I side of it. These states are the most similar (with the smallest order parameter value), but already labeled differently.

On the side of the CDW-I phase, the influence pattern is significantly different. The curvature of influential points corresponds to the growth of the order parameter,

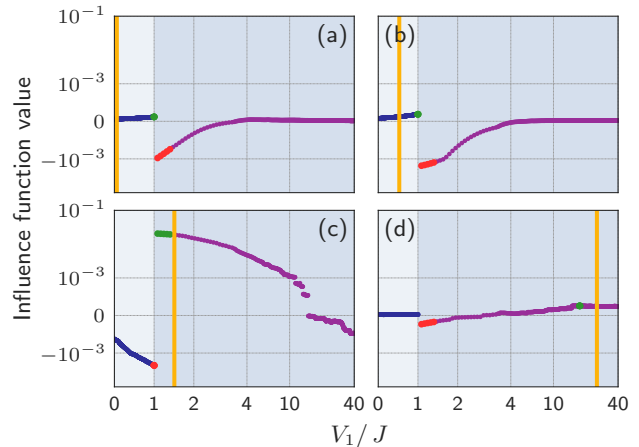


FIG. 2. Influence functions of all training examples i.e., ground states calculated for the transition line between LL and CDW-I for $V_2 = 0$ for chosen test points marked with an orange line. Blue dots are influence function values for training examples from the LL phase; purple ones are from the CDW-I phase. Larger green (red) dots are five the most influential helpful (harmful) training examples. The light grey background indicates V_1/J values of the LL phase, dark grey - the CDW-I phase. A symmetric log scale is used both in x and y axis with 3 and $|10^{-3}|$ chosen as threshold points, respectively.

and the most influential helpful points are the ones closest to the test point in the order parameter space, slightly shifted towards the transition point, as they provide more information. Panel (c) shows the influence functions of training points for the test states on the CDW-I side, close to the transition. The most harmful examples are, as in the previous test points, the ones closest to the transition, but on the other side of it. Panel (d), however, presents a distinct behavior of the most harmful examples being the closest to the transition, but on the same side. All the training points are similarly influential with small values of influential functions resulting in the almost flat line. It is a signature of the CNN's high certainty regarding the prediction made in panel (d) manifesting with a small test loss function $\mathcal{L}(z_{\text{test}}, \hat{\theta})$. Also, the analyzed test point is deeply in the CDW-I phase with all neighboring states being almost identical with the order parameter close to 1. The most harmful examples are the ones that are labeled as the CDW-I phase, but very different, so the ones closest to the transition.

The expected behavior of the most influential points indicates not only that the CNN correctly learned the order parameter, but also that this tool enables distinguishing between the phase transition types. In particular, the curvature of the line drawn by influence functions' values is different for the transitions characterized by continuous and discontinuous change of the order parameter.

Transfer learning. With a similar approach, we validate the transfer learning to another transition line. We take the trained CNN from Fig. 2 and in Fig. 3 we

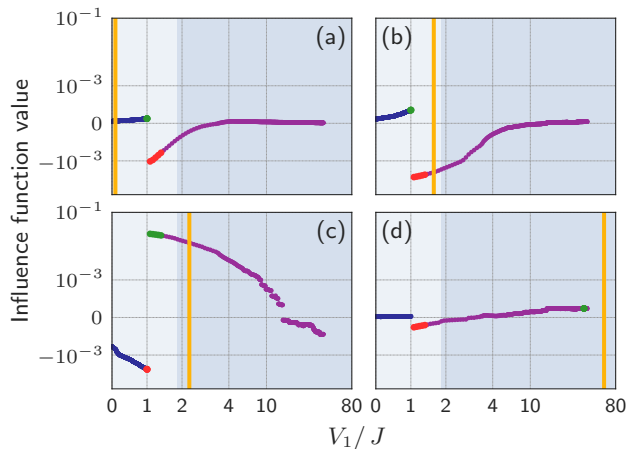


FIG. 3. Influence functions of all training examples i.e., ground states calculated for the transition line between LL and CDW-I for $V_2 = 0$ for chosen test states from transition line for $V_2 = 0.25 V_1$ marked with an orange line. Blue dots are influence function values for training examples from the LL phase for $V_2 = 0$; purple ones are from the CDW-I phase. Larger green (red) dots are five the most influential helpful (harmful) training examples. The light grey background indicates V_1/J values of the LL phase for $V_2 = 0.25 V_1$ line, dark grey - the CDW-I phase. A symmetric log scale is used both in x and y axis with 3 and $|10^{-3}|$ chosen as threshold points, respectively.

apply it to test states coming from the transition line for $V_2 = 0.25 V_1$, where the phase transition position is shifted to higher values of V_1/J . Therefore the training and test states come from different transition lines, $V_2 = 0$ and $0.25 V_1$, marked in Fig. 1(b) with the arrows (1) and (2), respectively.

Panels (a) and (b) of Fig. 3 show the influence function values of training data set for test states from the LL phase, while (c) and (d) - from the CDW-I phase. Due to the shifted transition point for the test line, compared to the training line, we see the same shift in the behavior of the most influential points on the CDW-I side. This shift corresponds to the fact that no longer the same value of V_1/J yields the same value of the order parameter, and that the ML algorithm still as the most influential points regards the states with the most similar order parameter.

Inferring the existence of the third phase. This time we analyze the transition line crossing three phases, LL, BO, and CDW-II, which is indicated by the arrow (3) in Fig. 1(b). Two order parameters are needed to describe this transition. One is the average difference of the next-nearest neighbor density, which equals zero in the LL and BO phases, and grows to 1 in the CDW-II phase. The other is the staggering of effective nearest-neighbor hoppings, being 0 in the LL phase, non-zero in the BO phase, and slowly decaying to 0 in the CDW-II phase. In the studied range of parameters, two phases (BO and CDW-II) co-exist (see appendix B). It is crucial to note that in this section, we train on the mentioned transition

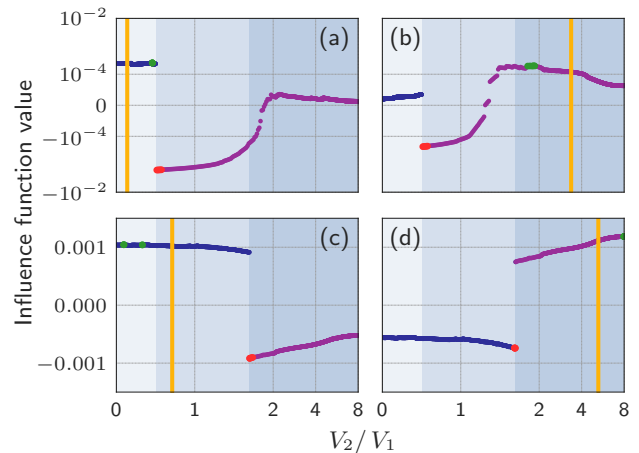


FIG. 4. Influence functions of all training examples i.e., ground states calculated for the transition line between LL, BO, and CDW-II for $V_1/J = 1$ labeled as (a)-(b) LL - not LL and (c)-(d) CDWII - not CDWII for chosen test points marked with an orange line. Blue dots are influence function values for training examples from (a)-(b) the LL phase, (c)-(d) the LL and BO phases, while purple ones (a)-(b) from the BO and CDW-II phases, (c)-(d) from the CDW-II phase. Larger green (red) dots are five the most influential helpful (harmful) training examples. The light background indicates V_1/J values of the LL, light grey - BO, and dark grey - CDW-II phase. In all subplots, a symmetric log scale is used in x axis with 2 chosen as a threshold point. A symmetric log scale with $|10^{-4}|$ as a threshold is used in y axis in panels (a)-(b), while in panels (c)-(d) the scale is linear.

line crossing three phases, but we label ground states only as belonging to one out of two phases.

In the first set-up, with results presented in the panels (a)-(b) of Fig. 4, we label ground states as belonging to the LL (blue dots, label 0) or belonging to the BO and CDW-II phases (purple dots, label 1). Independently on the test point location, within purple training points belonging to BO and CDW-II two similarity regions, understood as two groups of points with similar influence within the group, can be distinguished. The ML algorithm apparently learns two different patterns (order parameters) to classify the data correctly, and as such, it notices the existence of the third phase within the incorrectly labeled data. This would be impossible to notice without the use of interpretability methods, which in this sense pave the way towards unknown phases detection.

The second set-up consists of labeling the same data as belonging either to the LL and BO phases (blue dots, label 0) or to the CDW-II phase (purple dots, label 1). The influence functions values, resulting from this classification, are in the panels (c)-(d) of Fig. 4. The pattern they form is starkly different. First of all, no longer two similarity regions within training points from the LL and BO phases are distinguished. It is because this transition can be fully described with one order parameter, which is zero in the LL and BO phases, and non-zero in the CDW-

II phase. The behavior is then more similar to the one seen in Fig. 2 with the transition between LL and CDW-I. It is not identical, though, as in the phase LL+BO the most helpful training points are always distributed randomly, but deep in the LL phase, avoiding the BO phase. The most helpful points on the CDW-II side are also those deep in the CDW-II phase in contrast to Fig. 2, where they mostly follow the test point. The difference comes mostly from the fact that the deeper in the CDW-II phase, the smaller the BO order parameter, which is making CDW-II predictions less difficult. We claim that the observed pattern is the sign of not learning correctly the order parameter and potentially overfitting.

Finally, we trained a CNN on the same data, but with three labels correctly corresponding to all three phases. The influence patterns seen in Fig. 2 and panels (c)-(d) of Fig. 4 are repeated, indicating that CNN correctly learns both appropriate order parameters.

Conclusions. We used the influence functions, being the interpretability method aiming at approximating the LOO training, on the CNN trained to classify ground states of the extended 1D half-filled spinless Fermi-Hubbard model. We acknowledge significant finite-size effects, but we see that achieved results do not depend on the system size. We provided for the first time a strong indication that the ML algorithm indeed learned a relevant order parameter. Moreover, we showed that the influence functions, applied to the trained NN, were able to detect an unknown phase as well as distinguish between types of transitions. Two aspects impacted which training points were the most important for a given test point: how similar they were to the test state and how unique in the training data set. Together they gave a notion of distance or similarity used by the CNN in the phase classification problem and indicated that the pat-

terns relevant for the test states coincided with the order parameters.

The next step is to address open problems of topological models and MBL with NNs, whose logic can be finally discovered by influence functions. Even though this work concerned quantum phase transitions, this method may be easily applied to classical models as well. Moreover, influence functions proved to be very sensitive to outliers existing in the data set and may serve for anomaly detection. As such, it can be useful for analysis of experimental noise in the data on which various models are built and allow to judge how strongly it affects them.

Acknowledgements. An.D. acknowledges the financial support from the Polish National Science Centre within the Preludium grant No. 2019/33/N/ST2/03123. This project has also received funding from the European Unions Horizon 2020 research and innovation programme under the Marie Skłodowska-Curie grant agreement No. 665884 (P.H.). M.T. acknowledges the financial support from the Foundation for Polish Science within the Homing and First Team programmes co-financed by the EU Regional Development Fund. We also acknowledge the Spanish Ministry MINECO (National Plan 15 Grant: FISICATEAMO No. FIS2016-79508-P, SEVERO OCHOA No. SEV-2015-0522, FPI), European Social Fund, Fundaci Cellex, Fundaci Mir-Puig, Generalitat de Catalunya (AGAUR Grant No. 2017 SGR 1341, CERCA/Program), ERC AdG NOQIA, EU FEDER, MINECO-EU QUANTERA MAQS, and the National Science Centre, Poland-Symfonia Grant No. 2016/20/W/ST4/00314. Al.D. is financed by a Juan de la Cierva fellowship (IJCI-2017-33180).

-
- [1] J. Behler and M. Parrinello, *Generalized Neural-Network Representation of High-Dimensional Potential-Energy Surfaces*, *Phys. Rev. Lett.* **98**, 146401 (2007).
 - [2] L. Ward and C. Wolverton, *Atomistic calculations and materials informatics: A review*, *Curr. Opin. Solid State Mater. Sci.* **21**, 167 (2016).
 - [3] E. M. Christiansen *et al.*, *In silico Labeling: Predicting Fluorescent Labels in Unlabeled Images*, *Cell* **173**, 792 (2018).
 - [4] D. Wong and S. Yip, *Machine learning classifies cancer*, *Nature* **555**, 446 (2018).
 - [5] G. Carleo, I. Cirac, K. Cranmer, L. Daudet, M. Schuld, N. Tishby, L. Vogt-Maranto, and L. Zdeborová, *Machine learning and the physical sciences*, *Rev. Mod. Phys.* **91**, 045002 (2019).
 - [6] B. Naul, J. S. Bloom, F. Pérez, and S. van der Walt, *A recurrent neural network for classification of unevenly sampled variable stars*, *Nat. Astron.* **2**, 151 (2018).
 - [7] P. Baldi, P. Sadowski, and D. Whiteson, *Searching for exotic particles in high-energy physics with deep learning*, *Nat. Commun.* **5**, 4308 (2014).
 - [8] G. Torlai, G. Mazzola, J. Carrasquilla, M. Troyer, R. Melko, and G. Carleo, *Neural-network quantum state tomography*, *Nat. Phys.* **14**, 447 (2018).
 - [9] J. Carrasquilla, G. Torlai, and R. G. Melko, *Latent Space Purification via Neural Density Operators*, *Nat. Mach. Intell.* **1**, 155 (2019).
 - [10] G. Torlai and R. G. Melko, *Latent Space Purification via Neural Density Operators*, *Phys. Rev. Lett.* **120**, 240503 (2018).
 - [11] M. Bukov, A. G. R. Day, D. Sels, P. Weinberg, A. Polkovnikov, and P. Mehta, *Reinforcement Learning in Different Phases of Quantum Control*, *Phys. Rev. X* **8**, 031086 (2018).
 - [12] J. Carrasquilla and R. G. Melko, *Machine learning phases of matter*, *Nat. Phys.* **13**, 431 (2017).
 - [13] E. P. L. van Nieuwenburg, Y.-H. Liu, and S. D. Huber, *Learning phase transitions by confusion*, *Nat. Phys.* **13**, 435 (2017).
 - [14] F. Schäfer and N. Lörch, *Vector field divergence of predictive model output as indication of phase transitions*, *Phys. Rev. E* **99**, 062107 (2019).

- [15] A. Tanaka and A. Tomiya, *Detection of Phase Transition via Convolutional Neural Networks*, *J. Phys. Soc. Jpn.* **86**, 063001 (2017).
- [16] C.-D. Li, D.-R. Tan, and F.-J. Jiang, *Applications of neural networks to the studies of phase transitions of two-dimensional Potts models*, *Ann. Phys.* **391**, 312 (2018).
- [17] J. Liu, H. Shen, Y. Qi, Z. Y. Meng, and L. Fu, *Self-learning Monte Carlo method and cumulative update in fermion systems*, *Phys. Rev. B* **95**, 241104 (2017).
- [18] P. Broecker, J. Carrasquilla, R. G. Melko, and S. Trebst, *Machine learning quantum phases of matter beyond the fermion sign problem*, *Sci. Rep.* **7**, 8823 (2017).
- [19] P. Huembeli, A. Dauphin, P. Wittek, and C. Gogolin, *Automated discovery of characteristic features of phase transitions in many-body localization*, *Phys. Rev. B* **99**, 104106 (2019).
- [20] K. Ch'ng, N. Vazquez, and E. Khatami, *Unsupervised machine learning account of magnetic transitions in the Hubbard model*, *Phys. Rev. E* **97**, 013306 (2018).
- [21] H. Théveniaut and F. Alet, *Neural network setups for a precise detection of the many-body localization transition: finite-size scaling and limitations*, *Phys. Rev. B* **100**, 224202 (2019).
- [22] S. J. Wetzel, *Unsupervised learning of phase transitions: From principal component analysis to variational autoencoders*, *Phys. Rev. E* **96**, 022140 (2017).
- [23] K. Kottmann, P. Huembeli, M. Lewenstein, and A. Acin, *Unsupervised phase discovery with deep anomaly detection*, (2020), [arXiv:2003.09905 \[quant-ph\]](https://arxiv.org/abs/2003.09905).
- [24] D.-L. Deng, X. Li, and S. Das Sarma, *Quantum Entanglement in Neural Network States*, *Phys. Rev. X* **7**, 021021 (2017).
- [25] P. Huembeli, A. Dauphin, and P. Wittek, *Identifying quantum phase transitions with adversarial neural networks*, *Phys. Rev. B* **97**, 134109 (2018).
- [26] P. Zhang, H. Shen, and H. Zhai, *Machine Learning Topological Invariants with Neural Networks*, *Phys. Rev. Lett.* **120**, 066401 (2018).
- [27] Y.-H. Tsai, M.-J. Yu, Y.-H. Hsu, and M.-C. Chung, *Deep learning of topological phase transitions from entanglement aspects*, (2019), [arXiv:1909.04784 \[quant-ph\]](https://arxiv.org/abs/1909.04784).
- [28] E. Greplova, A. Valenti, G. Boschung, F. Schäfer, N. Lörch, and S. Huber, *Unsupervised identification of topological order using predictive models*, (2019), [arXiv:1910.10124 \[quant-ph\]](https://arxiv.org/abs/1910.10124).
- [29] X.-Y. Dong, F. Pollmann, and X.-F. Zhang, *Machine learning of quantum phase transitions*, *Phys. Rev. B* **99**, 121104 (2019).
- [30] L. Wang, *Discovering phase transitions with unsupervised learning*, *Phys. Rev. B* **94**, 195105 (2016).
- [31] R. A. Vargas-Hernández, J. Sous, M. Berciu, and R. V. Krems, *Extrapolating Quantum Observables with Machine Learning: Inferring Multiple Phase Transitions from Properties of a Single Phase*, *Phys. Rev. Lett.* **121**, 255702 (2018).
- [32] Y. Zhang and E.-A. Kim, *Quantum Loop Topography for Machine Learning*, *Phys. Rev. Lett.* **118**, 216401 (2017).
- [33] M. J. S. Beach, A. Golubeva, and R. G. Melko, *Machine learning vortices at the Kosterlitz-Thouless transition*, *Phys. Rev. B* **97**, 045207 (2018).
- [34] M. Richter-Laskowska, H. Khan, N. Trivedi, and M. M. Maška, *A machine learning approach to the Berezinskii-Kosterlitz-Thouless transition in classical and quantum models*, *Condens. Matter Phys.* **21**, 33602 (2018).
- [35] R. Guidotti, A. Monreale, S. Ruggieri, F. Turini, D. Pedreschi, and F. Giannotti, *A Survey Of Methods For Explaining Black Box Models*, [arXiv:1802.01933](https://arxiv.org/abs/1802.01933) (2018).
- [36] F. Doshi-Velez and B. Kim, *Towards A Rigorous Science of Interpretable Machine Learning*, [arXiv:1702.08608](https://arxiv.org/abs/1702.08608) (2017).
- [37] A. Baehrens, T. Schroeter, and S. Harmeling, *How to Explain Individual Classification Decisions*, *J. Mach. Learn. Res.* **11**, 1803 (2010).
- [38] M. T. Ribeiro, S. Singh, and C. Guestrin, *Why Should I Trust You? Explaining the Predictions of Any Classifier*, in *Proceedings of the 22nd ACM SIGKDD International Conference on Knowledge Discovery and Data Mining* (2016) pp. 1135–1144.
- [39] B. Zhou, A. Khosla, A. Lapedriza, A. Oliva, and A. Torralba, *Learning deep features for discriminative localization*, in *Proceedings of IEEE Conference on Computer Vision and Pattern Recognition* (2016) pp. 2921–2929.
- [40] R. R. Selvaraju, M. Cogswell, A. Das, R. Vedantam, D. Parikh, and D. Batra, *Grad-CAM: Visual Explanations from Deep Networks via Gradient-based Localization*, [arXiv:1610.02391](https://arxiv.org/abs/1610.02391) (2016).
- [41] A. Chattopadhyay, A. Sarkar, P. Howlader, and V. N. Balasubramanian, *Grad-CAM++: Improved Visual Explanations for Deep Convolutional Networks*, in *IEEE Winter Conf. on Applications of Computer Vision (WACV2018)* (2018).
- [42] Q. Zhang and S.-C. Zhu, *Visual interpretability for deep learning: a survey*, *Front. Inform. Technol. Electron. Eng.* **19**, 27 (2018).
- [43] EU General Data Protection Regulation (GDPR), *Regulation (EU) 2016/679 of the European Parliament and of the Council of 27 April 2016 on the protection of natural persons with regard to the processing of personal data and on the free movement of such data, and repealing Directive 95/46/EC (General Data Protection Regulation)*, *OJ L* **119/1** (2016).
- [44] T. Songül, *Fair and Unbiased Algorithmic Decision Making*, *JRC Tech. Rep.* **10** (2018).
- [45] C. Zhang, S. Bengio, M. Hardt, B. Recht, and O. Vinyals, *Understanding deep learning requires rethinking generalization*, in *International Conference on Learning Representation* (2017).
- [46] W. Brendel and M. Bethge, *Approximating CNNs with Bag-of-local-Features models works surprisingly well on ImageNet*, in *International Conference on Learning Representations* (2019).
- [47] R. D. Cook, *Detection of Influential Observation in Linear Regression*, *Technometrics* **19**, 15 (1977).
- [48] R. D. Cook and S. Weisberg, *Characterizations of an Empirical Influence Function for Detecting Influential Cases in Regression*, *Technometrics* **22**, 495 (1980).
- [49] R. D. Cook and S. Weisberg, *Residuals and Influence in Regression* (Chapman and Hall, New York and London, 1982).
- [50] P. W. Koh and P. Liang, *Understanding Black-box Predictions via Influence Functions*, in *Proceedings of the 34th International Conference on Machine Learning* (2017) pp. 1885–1894.
- [51] P. W. Koh, K.-S. Ang, H. H. K. Teo, and P. Liang, *On the Accuracy of Influence Functions for Measuring Group Effects*, [arXiv:1905.13289](https://arxiv.org/abs/1905.13289) (2019).
- [52] A. Dawid, P. Huembeli, M. Tomza, M. Lewenstein, and A. Dauphin, [http://doi.org/10.5281/zenodo.1111111](https://doi.org/10.5281/zenodo.1111111).

- 3746540 (2020), GitHub repository: Interpretable-Phase-Classification (Version arXiv1.0).
- [53] E. Hallberg, E. Gagliano, and C. Balseiro, *Finite-size study of a spin-1/2 Heisenberg chain with competing interactions: Phase diagram and critical behavior*, *Phys. Rev. B* **41**, 9474 (1990).
- [54] T. Mishra, J. Carrasquilla, and M. Rigol, *Phase diagram of the half-filled one-dimensional t - V - V' model*, *Phys. Rev. B* **84**, 115135 (2011).
- [55] P. Weinberg and M. Bukov, *QuSpin: a Python package for dynamics and exact diagonalisation of quantum many body systems part I: spin chains*, *SciPost Phys.* **2**, 003 (2017).
- [56] P. Virtanen et al., *SciPy 1.0: Fundamental Algorithms for Scientific Computing in Python*, *Nat. Methods* **17**, 261 (2020).
- [57] M. Lin, Q. Chen, and S. Yan, *Network in network*, (2013), [arXiv:1312.4400 \[cs.NE\]](https://arxiv.org/abs/1312.4400).

Appendix A: Convolutional neural network

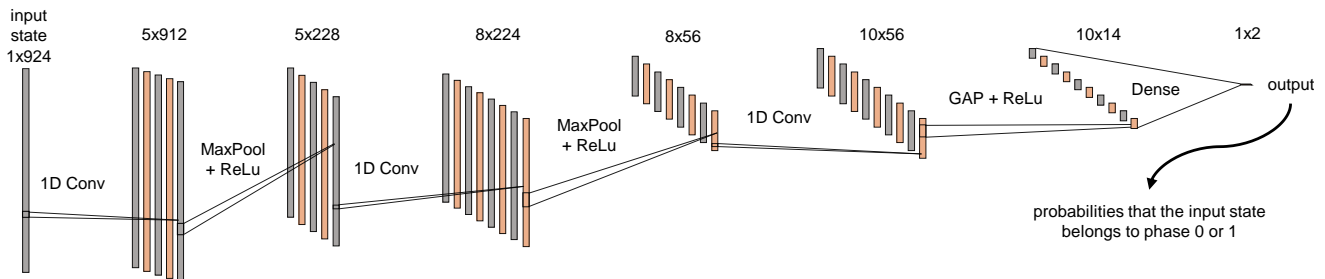


FIG. 5. Scheme of used architecture. Length scale does not apply.

We use a neural network (NN) (see Fig 5) consisting of 3 one-dimensional convolutional layers with 5 filters on the input vector, 8 filters on the first hidden layer and 10 filters for the last convolutional layer. After the first 2 convolutions we apply a max pooling layer to reduce the dimension, and the last convolutional layer is followed by a global average pooling (GAP) layer. The GAP architecture has been introduced in [57] and has found applications in discriminative localization of objects in image data [39]. It reduces each filter of the final convolution to a single value. After the GAP we have one fully connected layer with two output neurons that predict the labels. The GAP makes sure that most of the weights of the NN are contained in the convolutional part. We use this technique here to reduce the amount of weights in the fully connected part of the NN. For the training of the NN we use state vectors from each phase as an input and label them with 0 or 1 for each phase. The state vectors are obtained via exact diagonalization of the Hamiltonian B1.

We use L_2 regularization during the training to effectively decrease the certainty of the NN's predictions. Actually, the undertrained NN with imperfect accuracy can provide the better intuition behind the problem than overtrained one, whose predictions are impacted by overfitting. Used CNNs had accuracy between 89 and 96%.

For the results in Fig. 3 we apply transfer learning, which means that we use a NN that was trained with a training set that comes from a different domain than the test data. In our case the domains are different trajectories through the phase space indicated in Figure 1 with the arrows (1) and (2) where the phase transition appears for different values of V_1/J .

Appendix B: Phase diagram of the extended 1D half-filled spinless Fermi-Hubbard model

We study the 1D system consisting of spinless fermions at half filling with hopping between neighboring sites with amplitudes J , interacting with nearest neighbors with strength V_1 and next-nearest neighbors with strength V_2 :

$$\hat{H} = -J \sum_{\langle i,j \rangle} c_i^\dagger c_j + V_1 \sum_{\langle i,j \rangle} n_i n_j + V_2 \sum_{\langle\langle i,j \rangle\rangle} n_i n_j. \quad (\text{B1})$$

The model exhibits four different phases, two of them co-exist in the limited range of parameters. Without the next-nearest-neighbor interaction, V_2 , the system can follow only patterns of the gapless liquid Luttinger (algebraic) phase (LL) or the charge-density wave of the type I (CDW-I) with the degenerated density pattern 101010. The CDW-I order parameter describing this transition reads $O_{\text{CDW-I}} = \frac{1}{L} \sum_{\langle i,j \rangle} |n_i - n_j|$, where $\langle \rangle$ symbolizes nearest

neighbors. The next-nearest-neighbor interaction, V_2 competes with V_1 , so for non-zero V_2 but still smaller than V_1 the transition between LL and CDW-I shifts towards bigger V_1 . For sufficiently strong V_2 the bond-order (BO) phase emerges with the order parameter $O_{\text{BO}} = \frac{1}{L} \sum_i (-1)^i B_i$, where $B_i = \langle c_i^\dagger c_{i+1} + c_{i+1}^\dagger c_i \rangle$. It turns into the charge-density wave of the type II (CDW-II) with the degenerated density pattern 11001100 for large V_2 values, with $O_{\text{CDW-II}} = \frac{1}{L} \sum_{\langle\langle i,j \rangle\rangle} |n_i - n_j|$, where $\langle\langle \rangle\rangle$ symbolizes next-nearest neighbors.

To calculate the ground states and order parameters of the model, we use QuSpin package [55] to write the Hamiltonian for 12-site system in the Fock basis, resulting in 924 basis states. We assume periodic boundary conditions. The exact diagonalization is done with the SciPy package [56]. The ground states belonging to BO, CDW-I and II phases are degenerated. In order to lift the degeneracy, we apply symmetry breaking fields that favor one of the patterns. This approach results in non-zero corresponding order parameters independently of the phase, therefore we define transition points as such parameters of the system that correspond to the order parameter being 10 times bigger than the corresponding symmetry breaking fields. As such, due to the guiding fields of values 10^{-7} , 10^{-5} , and 10^{-4} for 101010 and 11001100 density patterns and 1010 hopping pattern, respectively, the order parameters of values 10^{-6} , 10^{-4} , and 10^{-3} signal the transition to the CDW-I, CDW-II, and BO phase, respectively. It is interesting to note that the results presented in this work stay the same without the symmetry breaking fields, and also do not depend on the size of the system.

Within this work we train the convolutional neural network on three transition lines indicated with arrows (1)-(3) in Fig. 1(b). The first transition line leads from the LL to the CDW-I phase, and is calculated for constant $V_2 = 0$ and $V_1/J = \langle 0, 40 \rangle$. It is a source of training data for both Figs. 2 and 3, and test data for Fig. 2. It is symbolized in Fig. 1(b) with the arrow (1), and the values of corresponding order parameter $O_{\text{CDW-I}}$ are plotted in Fig. 6(a). The transition, defined as above, occurs for $V_1/J = 1$. The second transition line is calculated for $V_2 = 0.25 V_1$ and $V_1/J = \langle 0, 80 \rangle$. Indicated with the arrow (2), it is the source of test data for Fig. 3. Corresponding order parameter CDW-I is plotted in Fig. 6(b), and the transition takes place for $V_1/J = 1.85$. Final transition line cuts three phases: LL, BO, and CDW-II. It is marked with the arrow (3) and provides both training and test data for Fig. 4. It is calculated for constant $V_1 = 1/J$ and $V_2 = \langle 0, 8 \rangle V_1$. Transition between LL and BO occurs for $V_2 = 0.51 V_1$, and between BO and CDW-II for $V_2 = 1.7 V_1$. It is important to notice that for the chosen range of parameters $V_2 = \langle 1.7, 8 \rangle V_1$, two phases co-exist what can be seen in Fig. 6(c).

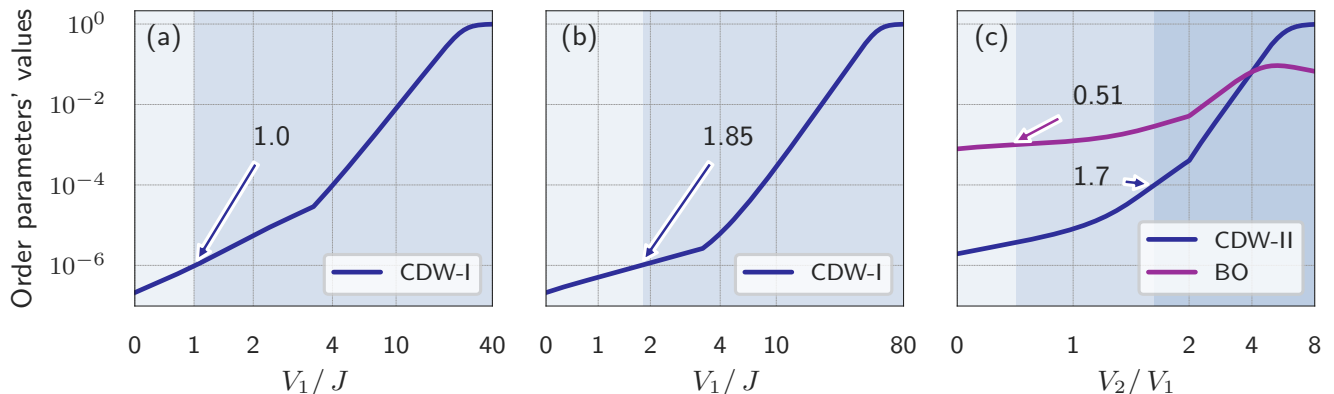


FIG. 6. Corresponding order parameters' values for three transition lines studied within this work, indicated with arrows (1)-(3) in Fig. 1(b). (a)-(b) CDW-I order parameter for the transition line between the LL and the CDW-I phase for $V_2 = 0$ and $0.25V_1$, respectively. (c) CDW-II and BO order parameters for the transition line between LL, BO, and CDW-II for $V_1 = 1/J$. Note the logarithmic scale of y -axis, and the symmetric log scale of x -axis with threshold points chosen to be 3, 3, and 2, respectively. Cusps in the lines are artificial and result from the symmetric log scale of x -axis.